Behavior of Shear Critical Wide Beams

by

Ivan Ornelas, B.S.C.E.

Departmental Report

Presented to the Faculty of the Graduate School of

The University of Texas at Austin

in Partial Fulfillment

of the Requirements

for the Degree of

Master in Science of Engineering

The University of Texas at Austin

December 2004

Behavior of Shear Critical Wide Beams

APPROVED BY
SUPERVISING COMMITTEE:

Oguzhan Bayrak, Supervisor

Eric B. Williamson, Reader

Dedication

To my family

Acknowledgements

The experience of working at the Ferguson Laboratory in the University of Texas at Austin has been one of the most valuable experiences that I have had in my life.

I would like to thank Dr. Oguzhan Bayrak for his tremendous support during the entire process of development of the project and after.

I would also like to thank Michael D. Brown, while I was under his supervision, I learned how to conduct a research project professionally and also to understand the different theoretical aspects involved during this study.

All of this research could not have been completed without the assistance of the staff at the Ferguson Structural Engineering Laboratory. I give my recognition to the technician. Blake Stasney, Michael Bell, and Dennis Fillip.

December 2004

Abstract

Behavior of Shear Critical Wide Beams

Ivan Ornelas, M.S.E.

The University of Texas at Austin, 2004

SUPERVISOR: Oguzhan Bayrak

Seven over-reinforced beams were tested at the Structural Engineering Ferguson Laboratory of The University of Texas at Austin. The main objective of this project was to determine the load capacity up to failure of every specimen and compare it with the nominal load capacity predicted by the STM provisions of the ACI 318-02 Code and AASHTO LRFD Bridge Design Specifications and determine the efficiency of these design codes.

Table of Contents

List of Tables

List of Figures

CHAPTER 1
INTRODUCTION

1.1 STRUT-AND-TIE MODELING

Strut-and-Tie Modeling (STM) is an ultimate strength design method based on the formation of a truss mechanism in cracked reinforced concrete members. Conventional analysis and design of concrete structures assumes that plane sections remain plane when they are subjected to stresses. This assumption is not always valid. The stress field in a concrete member can be non-linear due to disturbances within or applied to the member.

Such disturbances are due to the concentration of loads and changes in the geometry. Examples of each type of disturbance are shown in Figure 1.1 and Figure 1.2. The zones that are affected by such disturbances and present a nonlinear stress distribution are called “disturbed regions (D-regions)” and the regions where plane sections remain plane are called “Bernoulli regions (B-regions)”. Identification of a D-region is usually based on Saint Venant’s Principle which establishes that the strains produced in a body due to a system of forces in static equilibrium, are of negligible magnitude at a distance which is large compared with the linear dimensions of the member. This means that the effect of discontinuity on a D-region becomes negligible at a distance that is the approximate depth of the element.

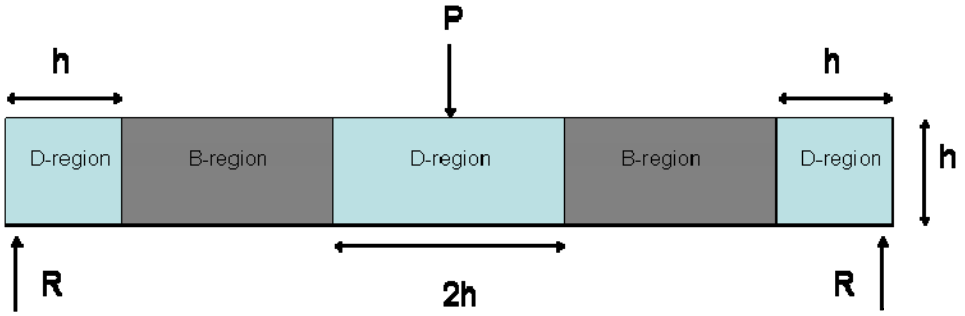

Figure 1.1 B- and D-regions due to applied loads

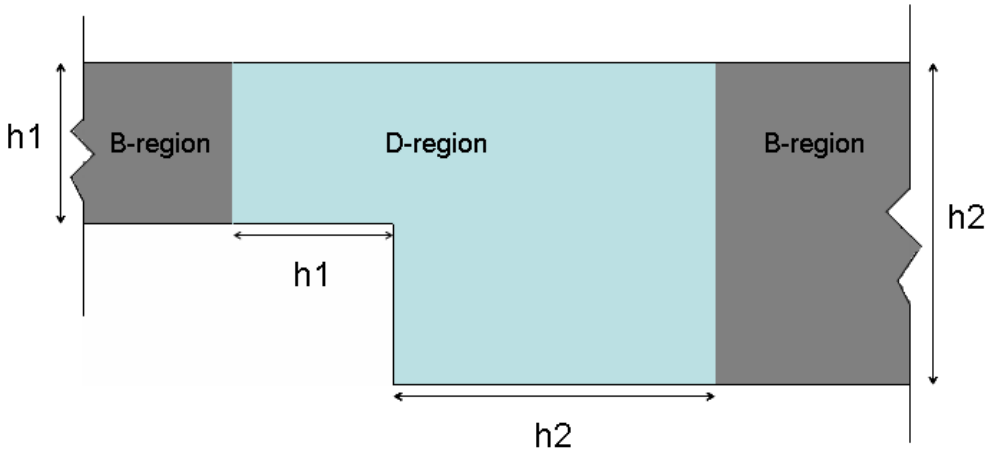

Figure 1.2 B- and D-regions due to geometric changes

Traditional methods of sectional analysis and design of reinforced concrete beams are based on the assumption that the beams behave entirely as B-regions. However, D-regions do not follow the assumptions used for the B-regions. Rules of thumb and past experiences have been traditionally used to design D-regions due to the lack of adequate theories to create an efficient and consistent method to design such members.

STM can be applied to D-regions based on converting the stresses in the member to forces in a strut-and-tie model. Loads applied to reinforced concrete produce a flow of stresses where the main trajectory of the compressive stresses (strut) forms after considerable cracking. Similarly, these compressive stresses are

interconnected by tensile stresses whose main trajectories can be used to identify ties.

STM is a method based on truss models, where only axial forces are transmitted by the struts and ties. The regions where the struts and ties intersect each other are important elements to consider in STM. Such regions are called the "nodal zones" or simply the nodes. Nodal zones have to be subjected to at least three forces to satisfy equilibrium. For example, CCC represents a node resisting three compressive forces (or struts), CTT and TTT nodes are also possible. Nodes also have finite dimensions (length, width, height). Node geometry can be determined by using a hydrostatic node definition where the faces of a node are perpendicular to the axes of the struts and ties that intersect at the node. The stresses acting on the faces of a hydrostatic node are equal.

1.2 HISTORICAL BACKGROUND

Ritter (1899) and Morsch (1902) were the first to introduce the concept of a truss model to interpret the behavior of reinforced concrete beams (Figure 1.3). A typical flexural member such as the one shown in Figure 1.3 is assumed to resist the tension force acting at the bottom of the beam and is assumed to behave like the bottom chord of a truss. The concrete compression zone at the top of the beam is assumed to act as the top chord. Inclined compressive struts and vertically oriented ties (stirrups) are used to model the shear transfer mechanism.

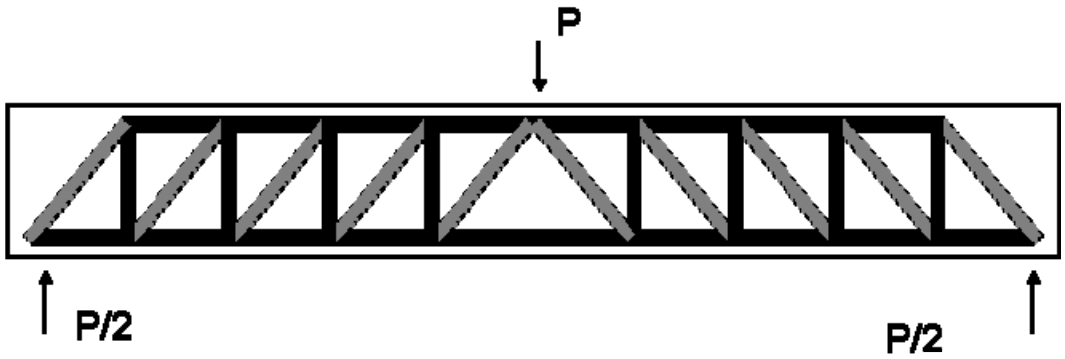

Figure 1.3 Truss model (Ritter and Mörsch)

During the 1960s, Thurliman, Marti and Mueller (Schalaich, Schäfer, Jennewein 1987) improved this model by applying the theories of concrete plasticity. Collins and Mitchell (1980's) introduced the effect of deformations on the truss model which could consider the effect of shear, torsion, bending and axial actions. The STM design procedure was introduced in the Canadian Code (CSA A 23.3-84) in 1984, AASHTO LRFD Bridge Design Specifications (section 5.6) in 1994 and ACI 318-02 (Appendix A) in 2002.

1.3 SCOPE OF THE PROJECT

This study focuses on examining the STM provisions of various design codes (ACI 318-02, AASHTO LRFD Bridge Design Specifications). In order to achieve this goal, seven specimens were tested in the Ferguson Structural Engineering Laboratory at the University of Texas at Austin. The capacities of the specimens were predicted using ACI 318-02 and AASTHO LRFD Bridge Design Specifications. These predictions facilitated the comparative evaluation of ACI 318-02 and AASTHO LRFD Bridge Design Specifications.

CHAPTER 2
Experimental Program

2.1 INTRODUCTION

The testing program included seven shear-dominated specimens (Beams 1 - 7). These specimens were divided into two sets based on their cross-sectional geometry (Figure 2.1). Data such as applied load, support reactions, deflections at mid-span, strains in flexural and shear reinforcement were recorded during the tests.

2.1 TEST SPECIMENS

The test specimens were of 14.5 feet long beams. Four of the seven specimens had 18-in. square sections and others had 18" x 30" sections. The amount of longitudinal reinforcement was kept constant at a reinforcement ratio of 2% for all specimens. Figure 2.1 shows the details of the test specimens.

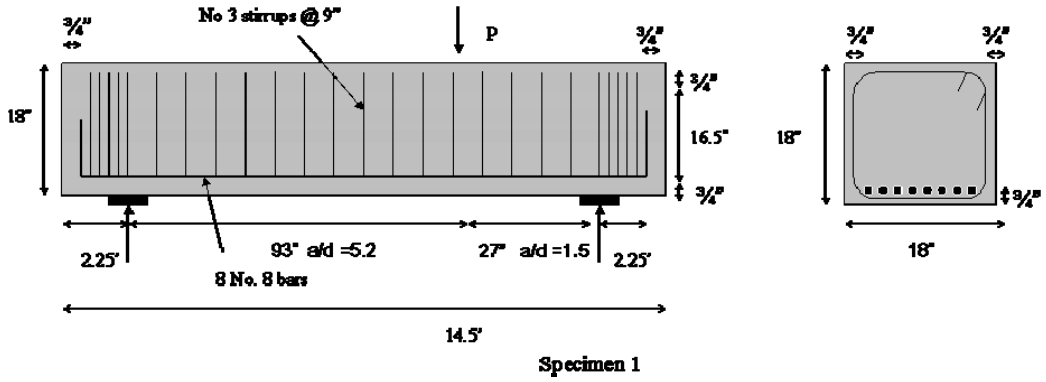

Figure 2.1 Test specimens

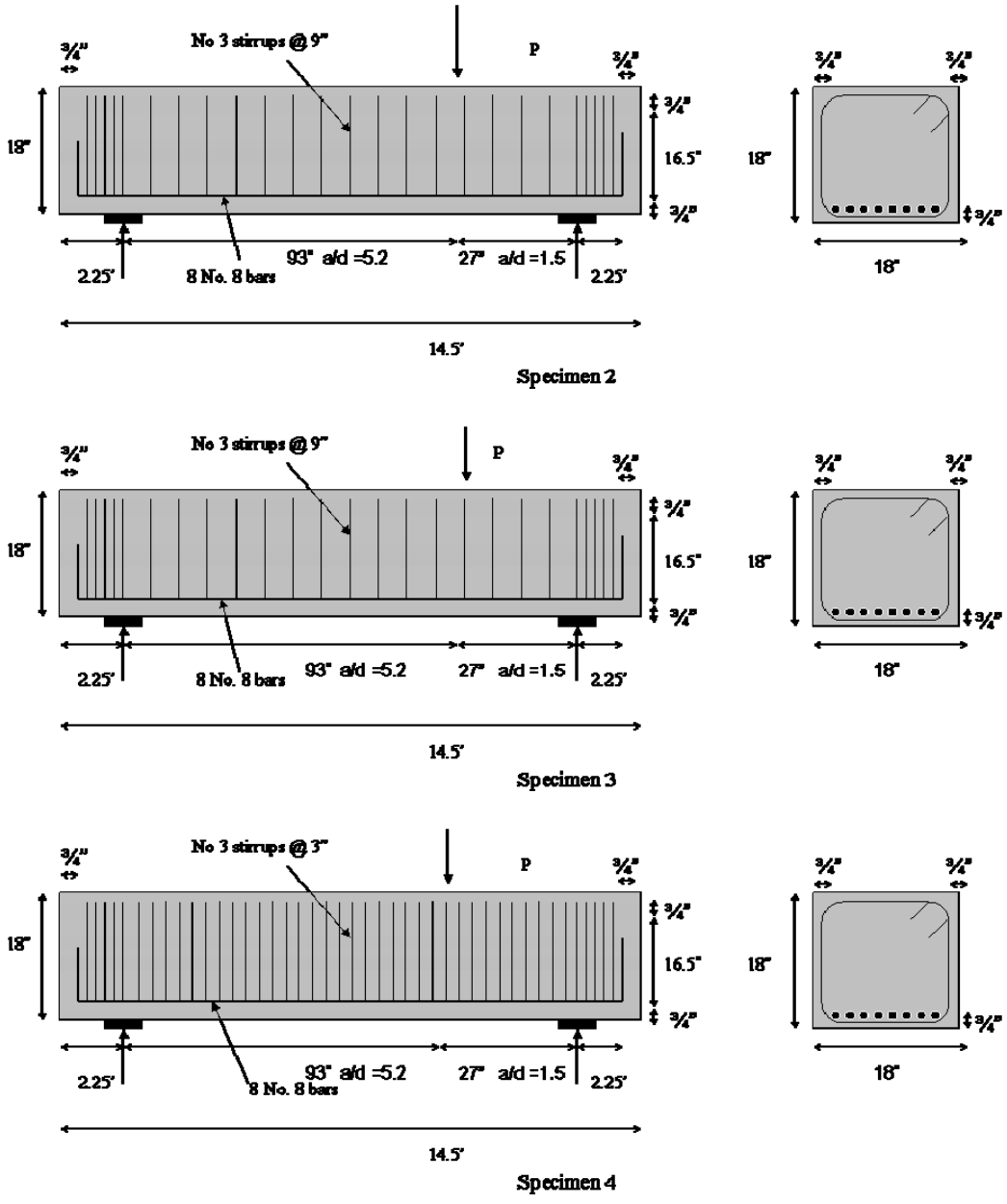

Figure 2.1 Test specimens (continuation)

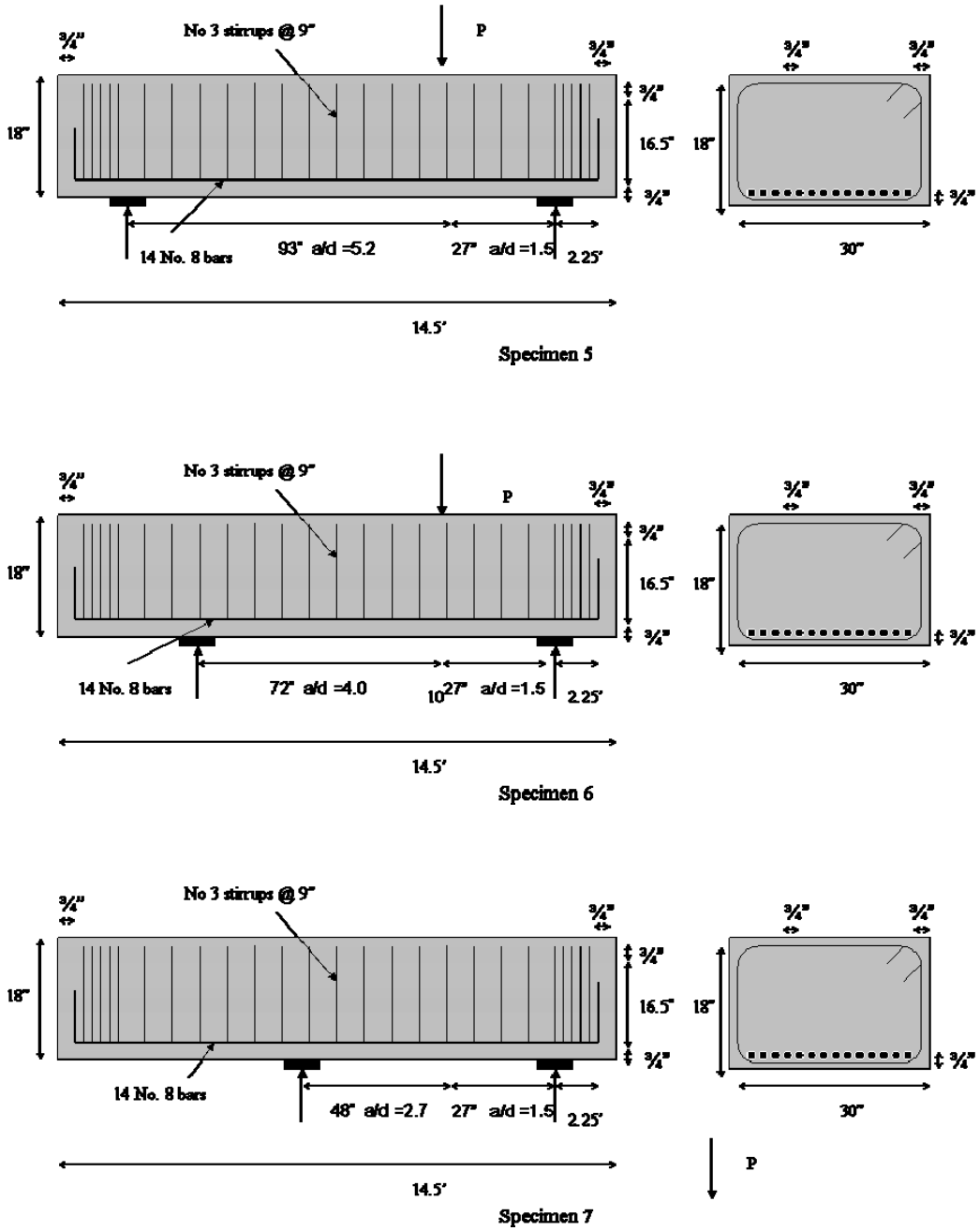

Figure 2.1 Test specimens (continuation)

2.2 TEST SET UP

Figure 2.2 shows the test setup used in the experimental investigation. A double acting hydraulic ram was used to apply the loads. The capacity of the test setup was 480 kips.

2.2.1 Frame

Figure 2.2 illustrates the test setup used in this study. The reaction frame was made up of W-shapes.

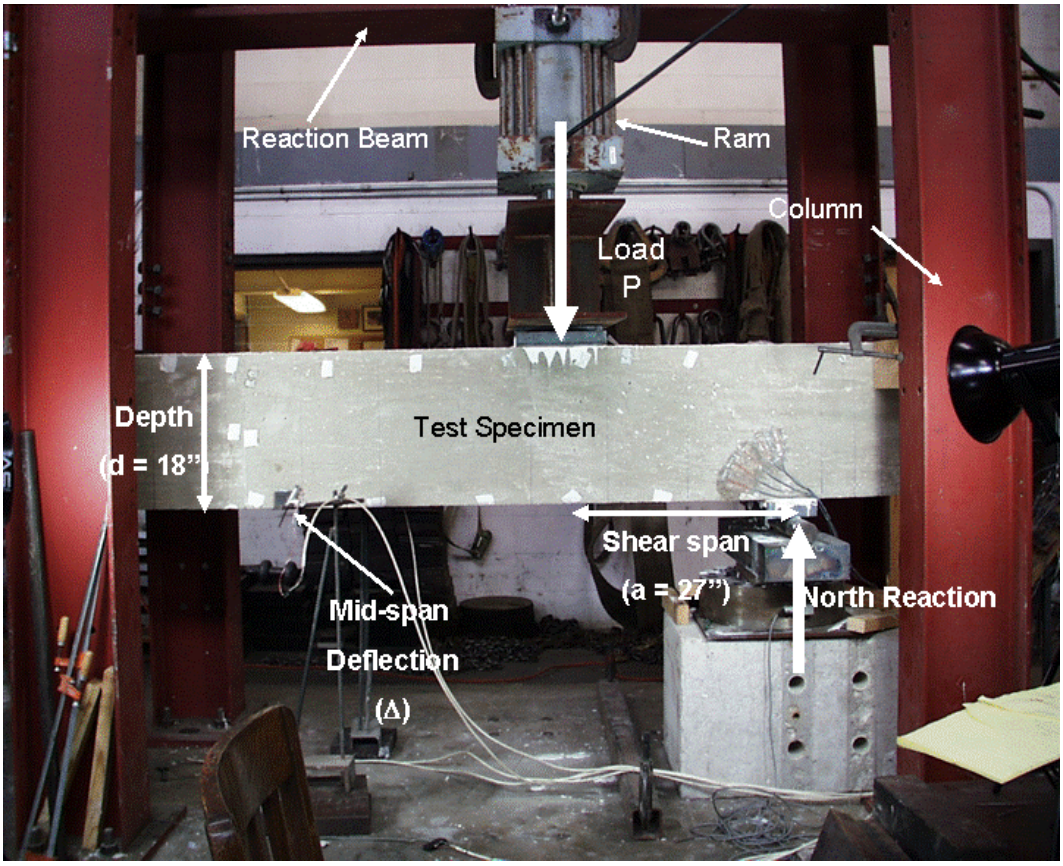

Figure 2.2 Test Setup

2.2.2 Supports and their accessories

Test specimens were simply supported. One of the supports represented a pinned support which restrained horizontal and vertical displacements and allowed rotations. The other support was a roller that permitted horizontal displacements and also rotations. Figure 2.3 shows the details of the supports used in this study.

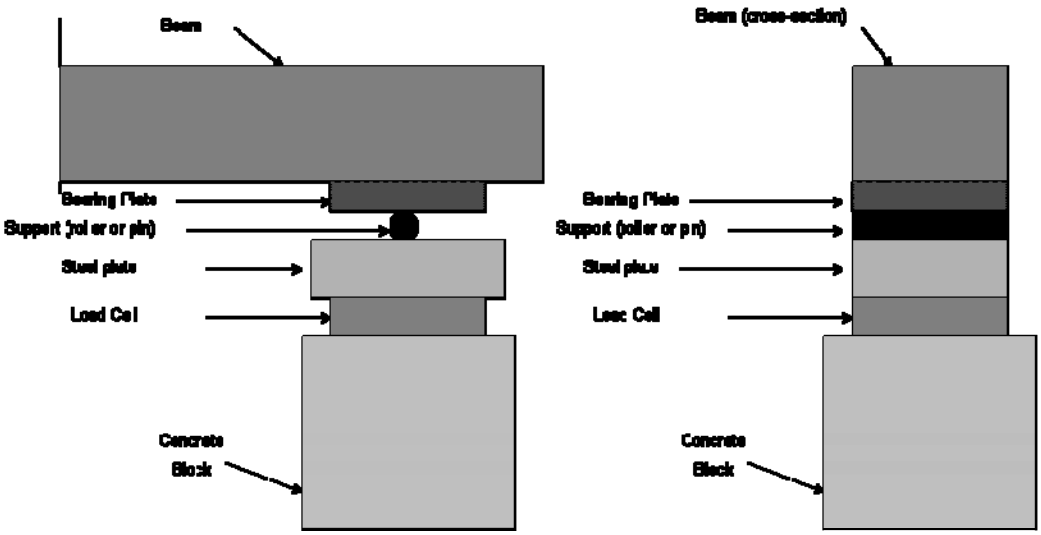

Figure 2.3 Supports

2.3 INSTRUMENTATION

2.3.1 Strain gages

Longitudinal bar strains were measured at two sections: one section at the point of maximum moment (the section under the load point) and the other section at one of the supports (North reaction in Figure 2.2).

In addition, stirrups were instrumented to measure the transverse strains. Strain gauges were attached on the surface of the concrete beam to measure compressive strains in the struts. These strain gauges were attached at varying

angles (30°, 45°, 60° measured from the horizontal axis) to capture the highest/most critical compressive strain (Figure 2.4).

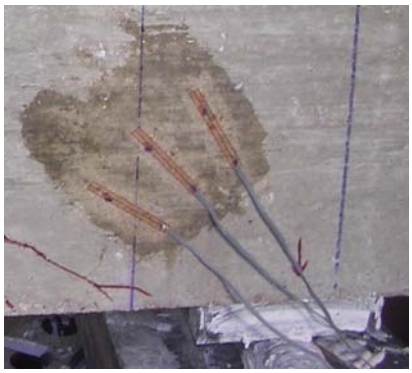

Figure 2.4 Strain gages on concrete

2.3.2 Potentiometers

Potentiometers were used to determine the vertical deflection of the beam at mid span (Figure 2.5).

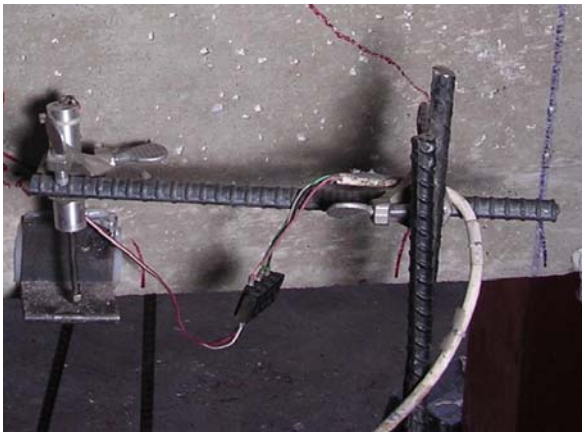

Figure 2.5 A typical Potentiometers

2.3.3 Data acquisition

Data from load cells, potentiometers, strain gauges and the loading ram were collected using an HP scanner.

2.4 CONSTRUCTION OF SPECIMENS

The formwork was constructed with ¾" plywood and 2" x 4" studs. The main objective in the construction of the formwork was to have a stiff formwork in order to prevent any significant movement during concrete casting. Before placing the reinforcing cages inside the formwork, the inner surface was lightly coated with form oil. Steel cages were placed in the formwork as shown in the following figures (Figure 2.4 and 2.5).

Figure 2.4 Cages placed in forms (set I)

Figure 2.5 Cages placed in forms (set II)

Then, concrete was poured (Figure 2.6 and Figure 2.7). Rod vibrators were used to reduce or eliminate the formation of voids. After concrete casting was completed the top surface of the formwork was covered with plastic (Figure 2.8).

Figure 2.6 Pouring of Concrete (set I)

Figure 2.7 Pouring of concrete (set II)

Figure 2.8 Plastic cover

2.5 MATERIAL STRENGTH

2.5.1 Compressive strength of concrete

All test specimens were cast at the same time in order to avoid variability in concrete strength. 6“ x 12” standard cylinders, cast along with the test

specimens, were tested (Figure 2.11) to determine the compressive strength of concrete at the time the test specimens were tested. The compressive strength of concrete of each test specimen, determined as the average of three cylinder tests, is given in Table 2.1.

Figure 2.9 Testing of compressive strength of concrete

Table 2.1 Geometric, reinforcement and material properties of test specimens

						Bearing Plate Dimension			
	Spec	Test No.	Section	Flexural Reinf.	Shear Reinf.	South Support	North Support	f'c (psi)	fy (Ksi)
Set I	1	1	18"x18"	8 No. 8	No. 3 @ 9"	10"x18"	2-6"x7.75"	2854	73
	2	2	18"x18"	9 No. 8	No. 3 @ 9"	10"x18"	6"x18"	2853	73
	3	3	18"x18"	10 No. 8	No. 3 @ 9"	10"x18"	6"x15.5"	2850	73
	4	4	18"x18"	11 No. 8	No. 3 @ 3"	10"x18"	6"x18"	2880	73
	4	5	18"x18"	12 No. 8	No. 3 @ 3"	10"x18"	6"x15.5"	2880	73
	2	6	18"x18"	13 No. 8	No. 3 @ 9"	10"x18"	6"x18"	2880	73
	1	7	18"x18"	14 No. 8	No. 3 @ 9"	10"x18"	6"x18"	3130	73
Set II	5	8	18"x30"	14 No. 8	No. 3 @ 9"	10"x18"	2-6"x7.75"	3107	73
	6	9	18"x30"	14 No. 8	No. 3 @ 9"	10"x18"	2-6"x7.75"	3572	73
	7	10	18"x30"	14 No. 8	No. 3 @ 9"	10"x18"	2-6"x7.75"	3646	73

2.5.1.1 Tensile strength of steel

Standard coupon tests were conducted on No. 8 bars (longitudinal steel) and No.3 bars (transverse bars) used in the test specimens. Yield strength of the No. 8 bars was 73 ksi.

CHAPTER 3
Test results

3.1 INTRODUCTION

The objective of this chapter is to describe the results from ten tests conducted on the seven specimens. Load history, deflections, reactions at supports, reinforcement strains, concrete strains, and test observations are described in the following sections.

3.2 SHEAR SPANS

In order to evaluate the influence of shear span-to-depth ratio on the behavior of test specimens, shear spans used in each test varied. Table 3.1 illustrates the shear span-to-depth ratio used in each test.

Table 3.1 Spans, North and South Shear spans

	Shear spans			Shear spans-to-depth ratio	
	Span (in)	North (in)	South (in)	North	South
Test 1	120	27	93	1.5	5.2
Test 2	120	27	93	1.5	5.2
Test 3	120	27	93	1.5	5.2
Test 4	120	27	93	1.5	5.2
Test 5	100	27	73	1.5	4.1
Test 6	100	27	73	1.5	4.1
Test 7	100	27	73	1.5	4.1
Test 8	120	27	93	1.5	5.2
Test 9	99	27	72	1.5	4.00
Test 10	75	27	48	1.5	2.7

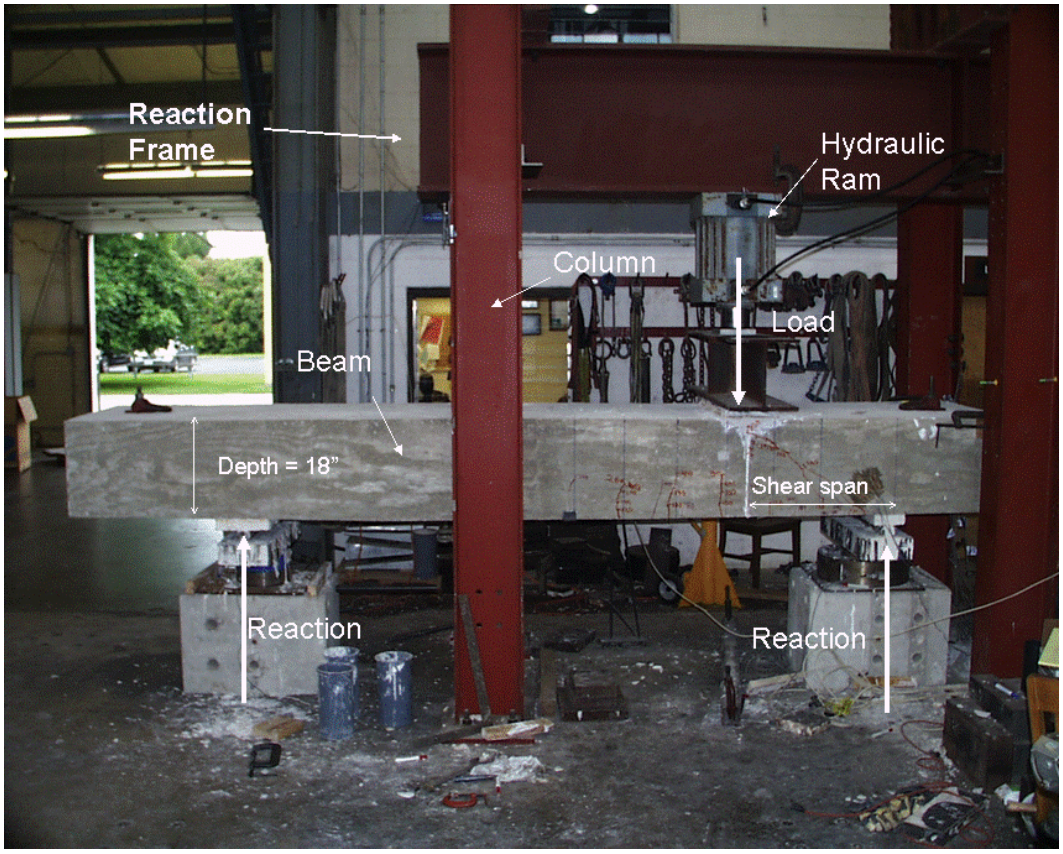

Figure 3.1 Configuration of tests (east view)

3.3 TEST OBSERVATIONS

A concentrated load (Figure 3.1) was applied to each test specimen and was increased gradually (at 5 kips load increments) until the test specimen failed.

The fist cracks to appear on both sides of the beam (east and west sides) were flexural and were located under the applied load. Then shear cracks were observed in the north end of the beam where there shear stresses were greater than those in the south end of the beam. These cracks appeared at different loads for each test specimen as shown in Table 3.2.

Table 3.2 Load at first cracking

	Flexural Cracks (Kips)	Shear Cracks (Kips)	
	East and Westside	East side	West side
Test 1	75	90	90
Test 2	65	90	80
Test 3	55	95	70
Test 4	55	80	80
Test 5	50	80	100
Test 6	60	100	100
Test 7	90	70	90
Test 8	100	160	160
Test 9	110	170	170
Test 10	110	200	200

Flexural cracks were observed on both sides at the same applied load and the pattern they followed were also the same on both sides. Both the length and width of the flexural cracks increased with increasing loads. In addition the number of flexural cracks observed also increased with progressively increasing loads.

The initial shear cracks were observed at slightly higher load levels than the flexural cracks. The crack patterns on both sides of the test specimens were similar.

3.4 CRACK PATTERN AT FAILURE

In specimens 1, 2, 4, 5, 6, and 7 shear failure took place in the short shear span (Figures 3.2, - 3.7). In test 8, 9 and 10 shear failure was observed in the long shear span (Figures 3.8 - 3.10). Failure of the test specimen 3 was different than all the other test specimens. Crushing of concrete adjacent to the loading plate and subsequent buckling of the compression bars was observed in this specimen. Figures 3.11 – 3.13 demonstrate the failure of the test specimens.

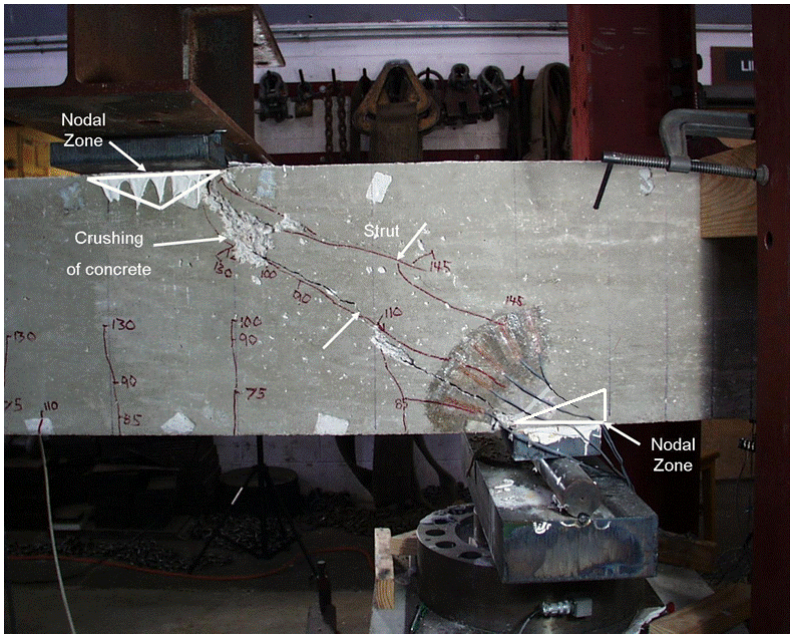

Figure 3.2 Failure of test specimen 1

Figure 3.3 Failure of test specimen 2

Figure 3.4 Failure of test specimen 4

Figure 3.5 Failure of test specimen 5

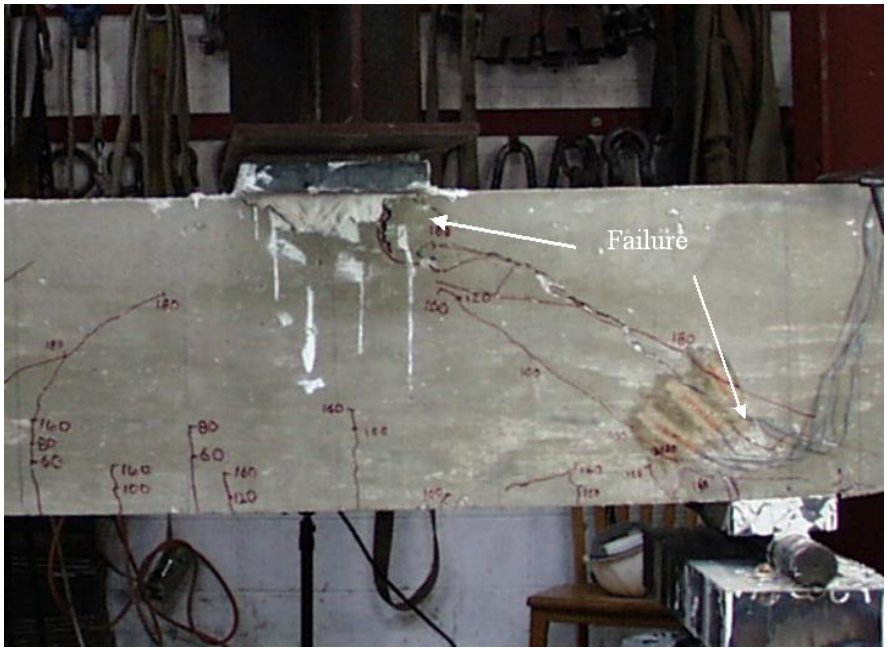

Figure 3.6 Failure of test specimen 6

Figure 3.7 Failure of test specimen 7

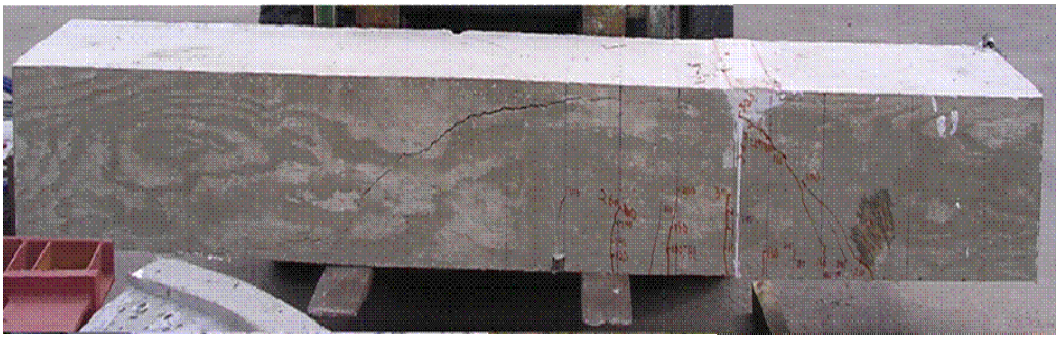

Figure 3.8 Failure of test specimen 8

Figure 3.9 Failure of test specimen 9

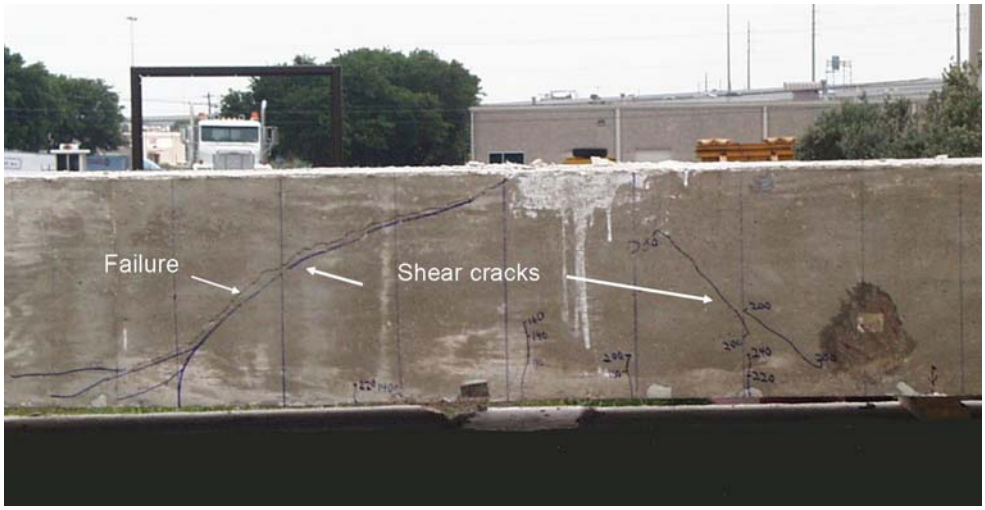

Figure 3.10 Failure of test specimen 10

In tests 8, 9 and 10 shear cracks that formed in the short shear span (north end of the test specimen) followed the same pattern observed in the previous seven tests. However, failure was marked by the formation of shear cracks in the long shear spans. These cracks formed suddenly.

The test specimen failed in a different manner during the third test. Although formation of the flexural cracks and subsequent shear cracks was similar to other specimens tested, the failure mode was different. The load capacity of the specimen was controlled by crushing of concrete adjacent to the loading plate. Figures 3.11-3.13 illustrate this phenomenon.

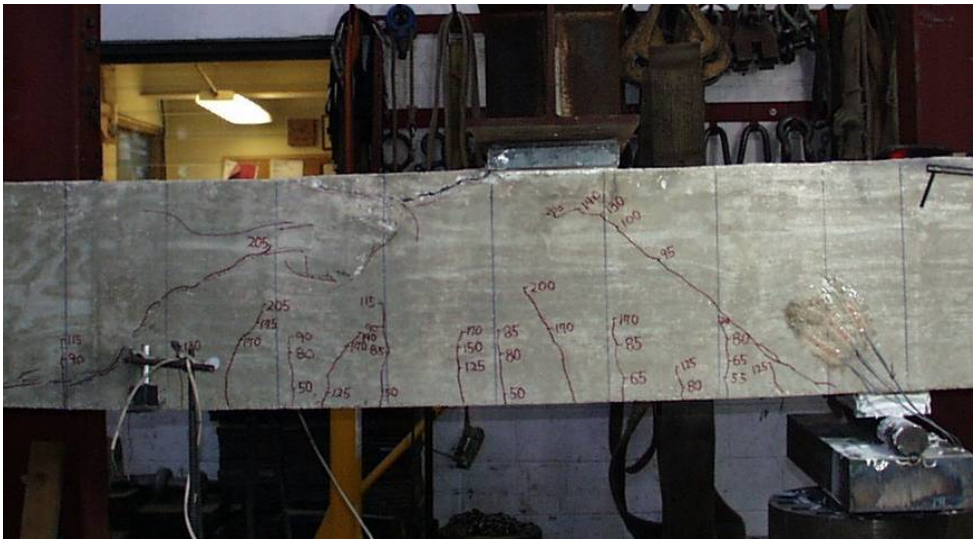

Figure 3.11 Failure of test specimen 3

Figure 3.12 Picture of the failure zone after removal of lose concrete

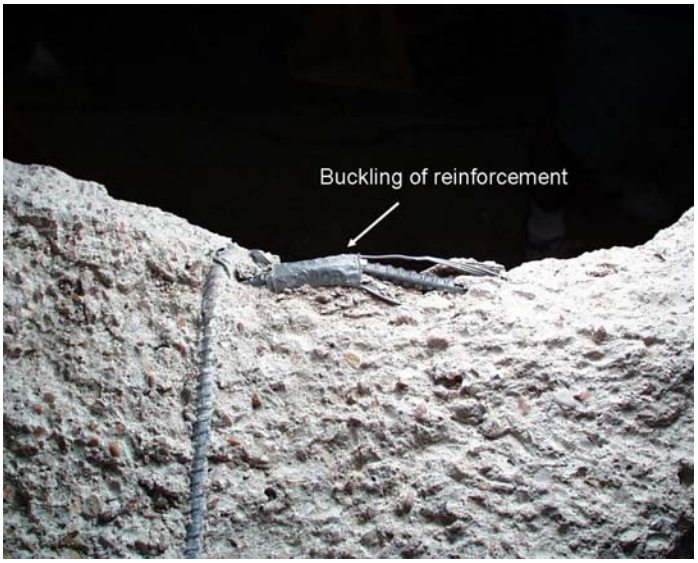

Figure 3.13 Buckling of compression reinforcement

3.5 LOAD VS. MIDSPAN DEFLECTION RESPONSE

Load vs. midspan deflection response of test specimens is given in Figure 3.14. Strain gauges installed on flexural reinforcement at critical sections (maximum moment section and at the north support) indicated that rebars did not yield.

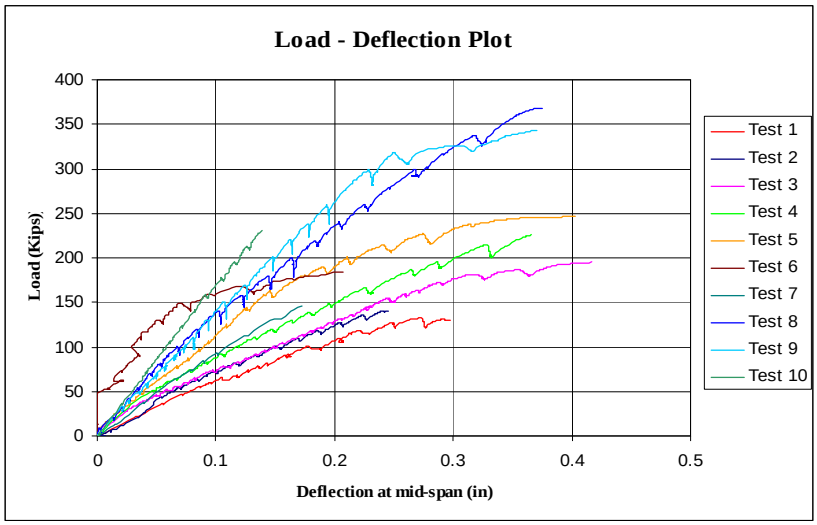

Figure 3.14 Load – Deflection of specimens

Table 3.3 illustrates the maximum deflection measured at the mid-span of each beam. As can be seen in this table, deflections measured at failure were small relative to span length

Table 3.3 Deflection at failure of specimens

	Tests									
	1	2	3	4	5	6	7	8	9	10
Δ (in)	0.30	0.25	0.42	0.37	0.40	0.21	0.17	0.37	0.37	0.14
Δ / L x 1000	2.5	2.0	3.5	3.1	4.0	2.1	1.7	3.1	3.7	1.8

3.6 CONCRETE STRAINS

The concrete strains at the north support were measured at three different angles: 30º, 45 º and 60º (Figure 3.15). A typical concrete strain load relationship is shown in Figure 3.16.

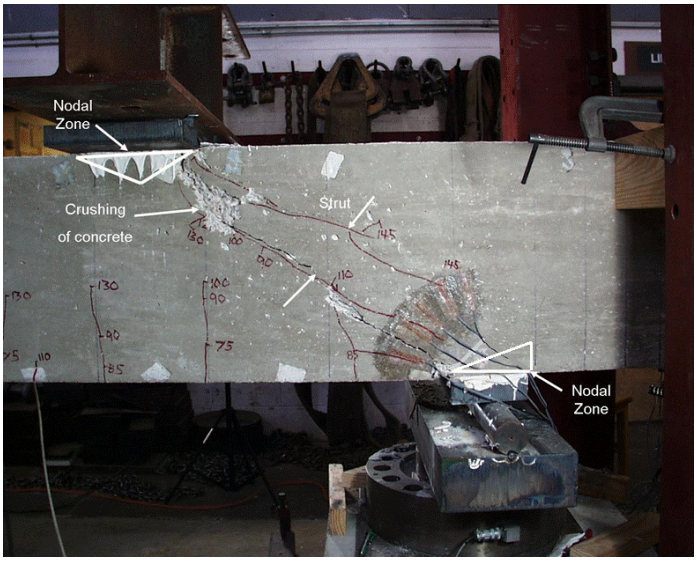

Figure 3.15 Strain gauges attached to the concrete

As can be seen in Figure 3.15 the inclination of the strut that formed between the applied load and the shape support is about 30º.

In other words the strain gauge applied at 30º degrees was essentially parallel to the shear cracks shown in Figure 3.15.

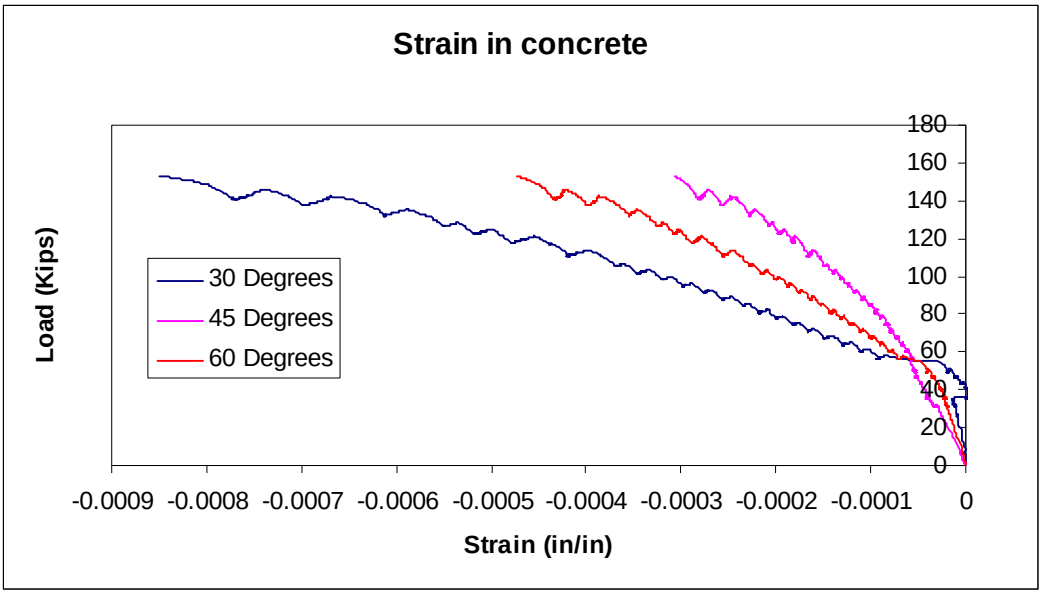

Figure 3.16 Concrete strain vs load relationship at the north support

In cases where the specimen failed in the short shear span (tests 1, 2, 4, 5, 6 and 7) maximum compressive strains were measured by the strain gauges that followed the axis of the strut that formed between the load point and the north support. Hence concrete gauges were instrumental in confirming the assumed strut and tie models.

CHAPTER 4
Significance of Test Results

4.1 INTRODUCTION

In this chapter load carrying capacity of the test specimens are calculated using Appendix A of ACI 318-02 STM provisions and chapter 5 of AASHTO LRFD Bridge Design Specifications. These predictions are compared with the experimental values to examine the accuracy and conservativeness of the relevant code provisions.

4.2 STRUT AND TIE MODELING PROVISIONS

In developing a strut-and-tie model, B-regions and D-regions need to be identified. D-regions are regions in which the "plane sections remain plane" assumption does not apply. Static or geometric discontinuities can be used to identify disturbed regions of a structure. In a geometrically uniform beam such as those used in this study, D-regions can be identified using St. Venant's principle. Figure 4.1 illustrates this concept.

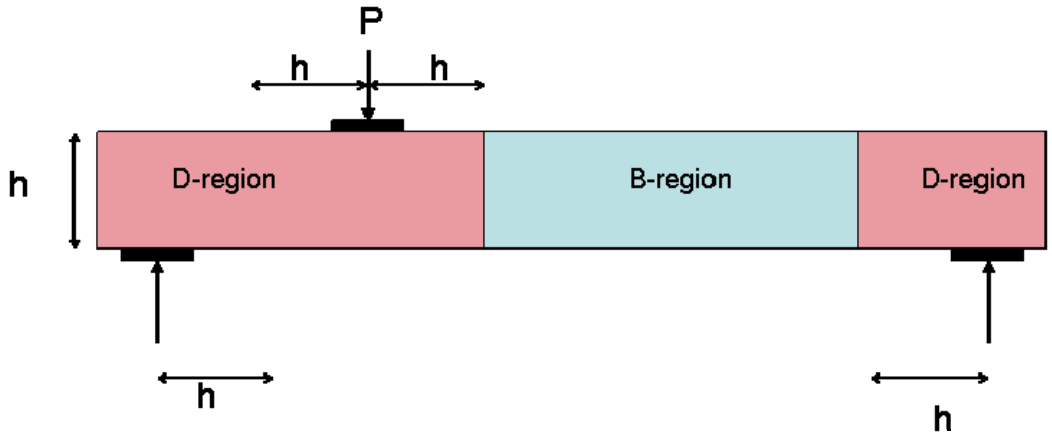

Figure 4.1 B- and D- Regions

Loads applied on a beam are transferred to the support by forming stress trajectories that can be used to determine the arrangement and orientation of the struts and ties (Figure 4.2).

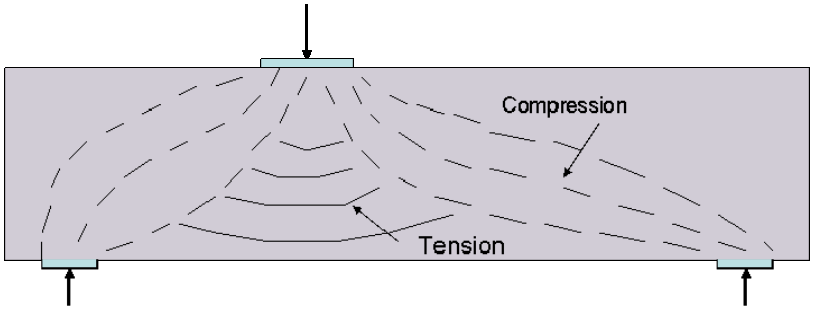

Figure 4.2 Stress flow

Stress trajectories (Figure 4.2) can be used to establish a truss mechanism as shown in Figure 4.3. The truss mechanism can be used to visualize the mechanism of load transfer from the points of load application to the supports. At the same time, the idealized truss can be designed and detailed to resist the applied loads in a safe manner.

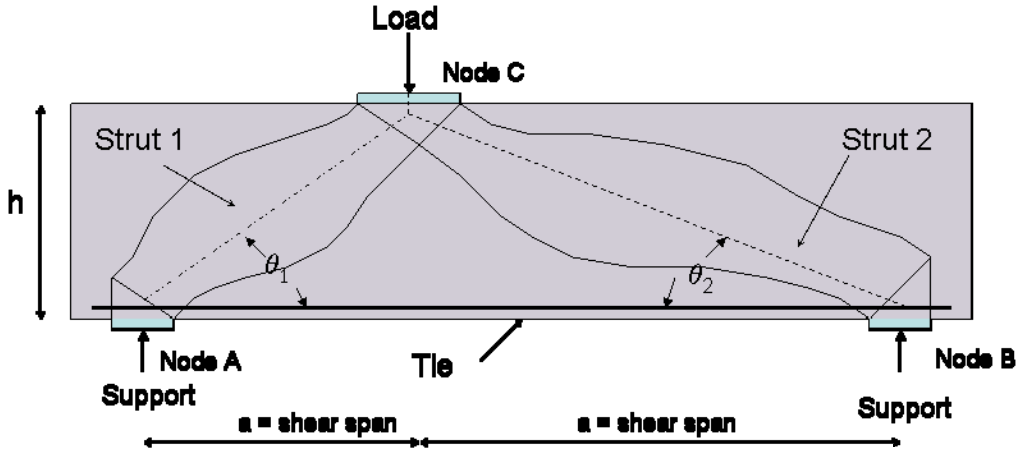

Figure 4.3 Strut and Tie model

The STM design procedure that is outlined in Appendix A of ACI-318 02 is based on the following relationship:

$$\phi F_n \geq F_u \qquad \text{(Equation 4.1)}$$

where,

ϕ = strength reduction factor

F_n = nominal strength of the strut, tie, or nodal zone

F_u = factored force acting in a strut, tie, bearing area, or nodal zone.

Then, the nominal strength of these elements (F_n) can be evaluated as a function of their geometry and material properties to resist the forces acting on them.

4.2.1.1 Strength of Nodal Zones

The nodal zone is defined by ACI 318-02 as a volume of concrete around a node that is assumed to transfer the strut-and-tie forces through the node. The node geometry is a function of the length of bearing plates (l_b) where the point loads or support reactions are located (when bearing plates are provided for these forces), the effective tie width (w_t), and the effective strut width (w_s).

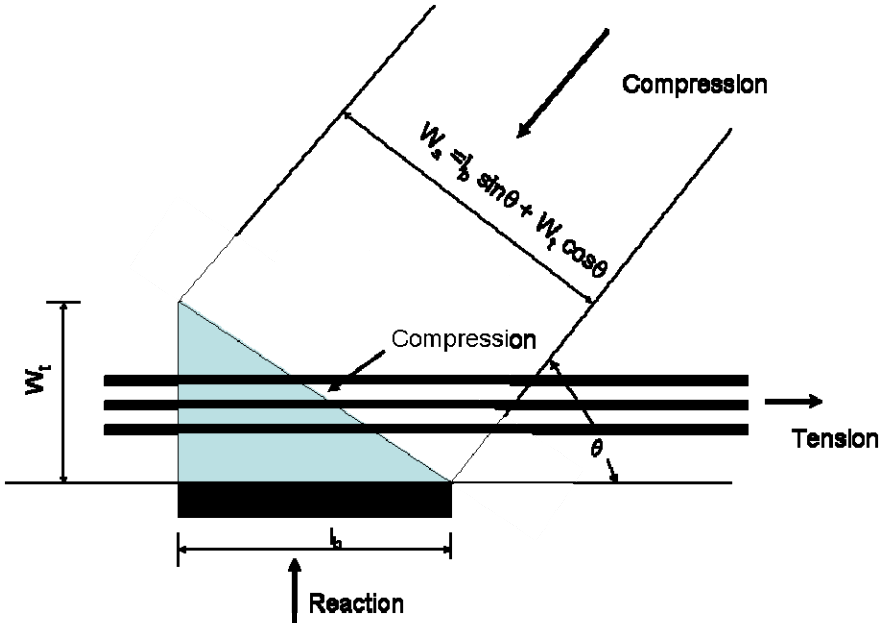

Figure 4.4 Extended Nodal Zone: CCT Node

Hydrostatic nodes can be used for any nodal zone which is not limited by bearing plates.

The strength of nodal zones can be determined by:

$$F_{nn} = f_{cu} * A_n \qquad \text{(Equation 4.2)}$$

where,

F_{nn} = nominal strength of a face of a nodal zone

f_{cu} = effective compressive strength of the concrete in the nodal zone

$$f_{cu} = 0.85 * \beta_n * f'_c \qquad \text{(Equation 4.3)}$$

where,

β_n = factor to account for the effect the anchorage of ties on the effective compressive strength of a nodal zone.

$\beta_n = 1.0$ for nodal zones bounded by struts or bearing areas

$\beta_n = 0.80$ for nodal zones anchoring one tie

$\beta_n = 0.60$ for nodal zones anchoring two or more ties

f'_c = specified compressive strength of the concrete

A_n = area of the face of the nodal zone where F_u acts

4.2.1.2 Strength of Struts

A strut is defined by ACI 318-02 as a compression member in a strut-and-tie model. Strut geometry is a function of the tie width (w_t), the width of bearing plate (l_b), and the angle of inclination (θ) as shown in Figure 4.4.

For struts that end at nodes which are not bordered by bearing plates, it is difficult to determine their widths. This width is not specified in the code. Finding the exact width of the compression zone delimited by the neutral axis and the border of the section may also become complex for the D-regions. Having recognized these difficulties, the strengths of the struts can be determined using the following expression:

$$F_{ns} = f_{cu} * A_c \qquad \text{(Equation 4.4)}$$

where,

F_{ns} = nominal strength of a strut

f_{cu} = effective compressive strength of a strut

$$f_{cu} = 0.85 * \beta_s * f'_c \qquad \text{(Equation 4.5)}$$

β_s = factor to account for the effect of cracking and confining reinforcement on the effective compressive strength of the concrete in a strut:

β_s = 0.75 if A.3.3 of ACI 318-02 is satisfied

β_s = 0.60 if A.3.3 of ACI 318-02 is not satisfied

Where section A.3.3 of ACI can be expressed as:

$$\sum \frac{A_{si}}{b * s_i} * \sin(\gamma_i) \geq 0.003 \qquad \text{(Equation 4.6)}$$

A_{si} = is the total area of reinforcement at spacing s_i

s_i = spacing of reinforcement

γ_i = angle between the axis of a strut and the bars in the i^{th} layer of reinforcement crossing that strut

b = width of beam

A_c = cross-sectional area at one end of the strut.

4.2.1.3 Strength of Ties

A tie is defined by ACI 318-02 as a tension member in a strut-tie-model. Ties are either longitudinal or transverse reinforcement subjected to tension.

The strength of a tie is defined by:

$$F_{nt} = A_{st} * f_y \quad \text{(excluding prestressed reinforcement)} \qquad \text{(Equation 4.7)}$$

where,

F_{nt} = nominal strength of a tie

A_{st} = area of nonprestressed reinforcement in a tie

f_y = specified yield strength of nonprestressed reinforcement

4.2.2 Calculations and Observations

In this section, capacities of the test specimens are calculated and computed capacities are compared with the experimental values. In this way, the conservativeness of the ACI 318-02 provisions are evaluated.

4.2.2.1 Nodal zones

Fisrt, the support reactions of the statically determinate test specimens are calculated. Subsequently, the following three forces can be determined:

F_{nn} = nominal strength of node at a face of a nodal zone

P_n = nominal force of specimen at failure of node

P_{test} = maximum load at failure of specimen obtained from test

Nodes A, B, and C are identified in Figure 4.5.

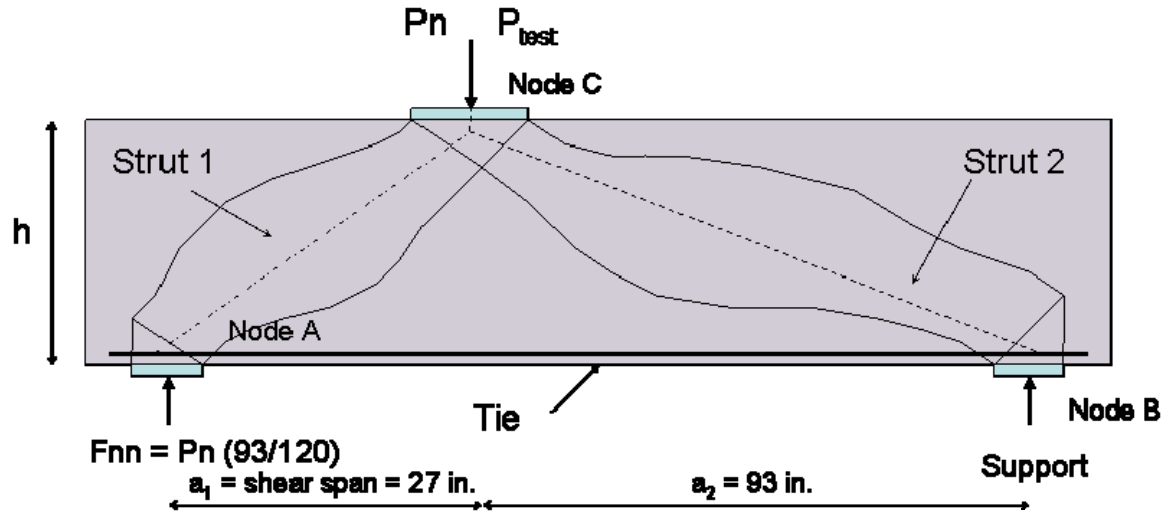

Figure 4.5 Nodal strengths

The strength of Node A of test specimen 1 (Figure 4.5) can be calculated as follows:

$f_{cu} = 0.85 * \beta_n * f'_c$

$\beta_n = 0.8$ for nodal zones anchoring one tie

$f_{cu} = 0.85 * 0.8 * 2.584 = 1.94$ ksi.

$Ac = 15.5"*6" = 93 \ in^2$ (area of bearing plate)

Therefore:

$F_{nn} = 1.94 * 93 = 180.5$ kips

(93/120) $P_n = F_{nn} = 180.5$ kips (see figure 4.5)

$P_n = 232.9$ kips

The same procedure is followed to evaluate F_{nn} and P_n of the other nodes (B and C) and the nodes of the other test specimens.

4.2.2.2 Struts

The following three forces are to be determined for the struts

F_{ns} = nominal compressive strength of a strut

P_n = external load force resulting in a strut force on F_{ns}

P_{test} = maximum load at failure of specimen obtained from a test

Struts 1 and 2 are identified in Figure 4.6

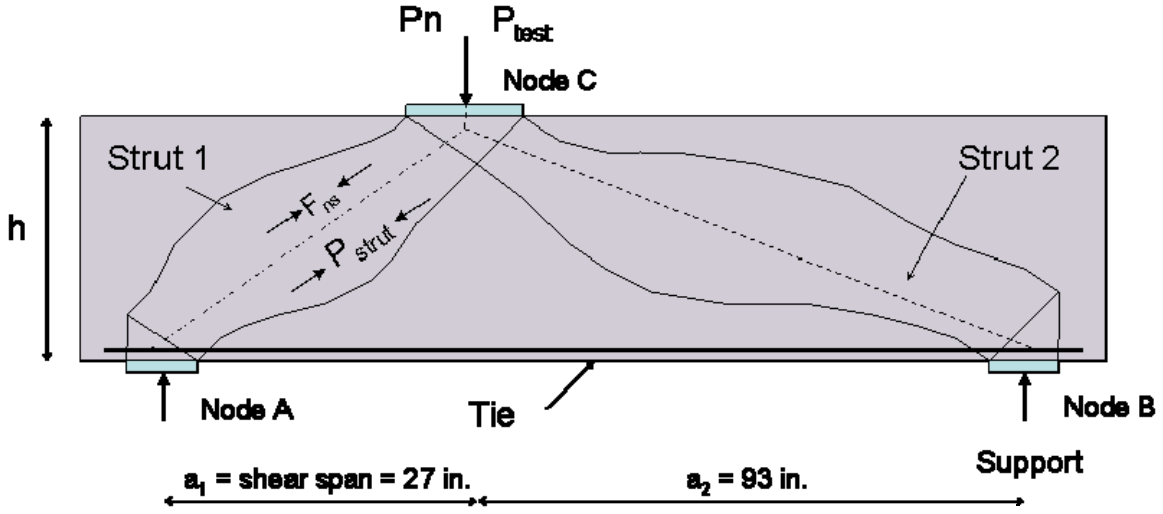

Figure 4.6 Strut strengths

The nominal strength of strut 1 of specimen 1 can be calculated as follows:

$F_{ns} = f_{cu} * A_c$

$Ac = W_s * A_c$ = the mazimum cross-section area of a bottle shaped strut

$w_t = \phi_{bar} + 2*(cover + \phi_{strirrup}) =$ width of the tie (see Figure 4.4)

$\phi_{bar} = 1$ in. cover = 0.75 in. $\phi_{stirrup} = 0.375$ in.

$w_t = 1" + 2*(3/4" + 3/8") = 3.25"$

$w_s = w_t*\cos(\theta) + l_b*\sin(\theta)$ = width of strut (see Figure 4.4)

$w_s = w_t * \cos(0.545) + l_b * \sin(0.545) = 5.9$ in.

b = 18" = width of the beam

$A_c = 5.89"*18" = 106.0$ in.^{2}

$f_{cu} = 0.85*\beta s*fc'$

$A_{si} = 0.22$ in.^{2}

$\sum \frac{Asi}{b*si} * \sin(\gamma i) = \frac{0.22}{18*9} * \sin(\pi/2 - \theta) = 0.0011$ this does not satisfy A.3.3

Therefore $\beta s = 0.60$

$f_{cu} = 0.85*0.6*2.854 = 1.46$ ksi

Therefore:

$F_{ns} = 1.455*106.02 = 154.3$ Kips

P_{strut} = load carried by the strut = (12/93) * sin(θ) * P_n (see figure 4.6)

$P_{strut} = 1.494\ P_n = F_{ns} = 154.32$ kips

$P_n = 103.3$ kips

The same procedure is followed to evaluate F_{ns} and P_n of strut 2 and the struts in the other test specimens:

4.2.2.3 Ties

The following three forces were determined for the tie

F_{nt} = nominal tensile strength of a tie

P_n = load carrying capacity of a test specimen as controlled by the capacity of a strut

P_{test} = load at failure of specimen obtained from test

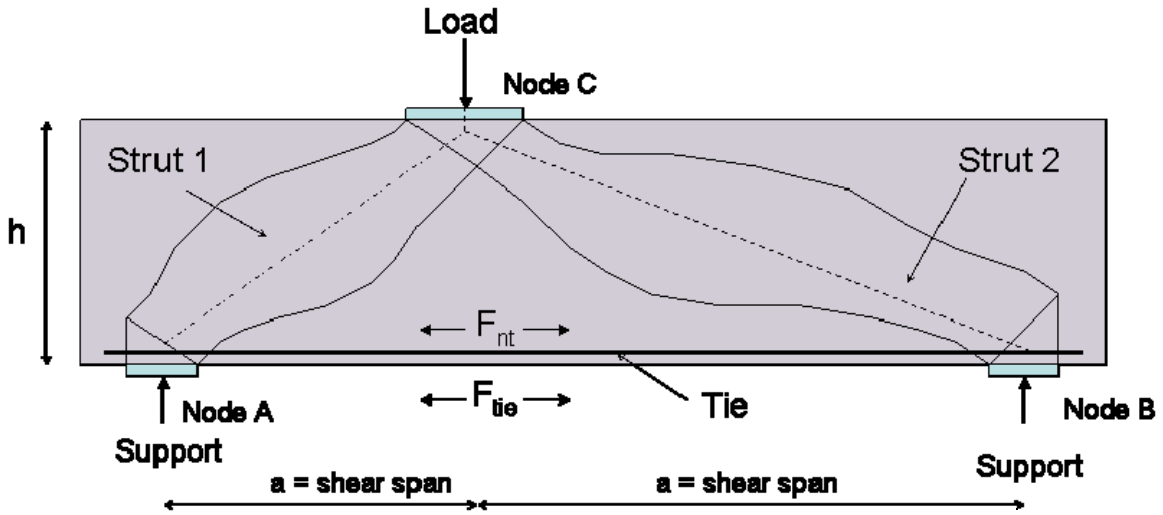

Figure 4.7 Tie strength

The tie strength of specimen 1 is calculated as follows:

$F_{nt} = A_s * fy$

$A_s = 6.28$ in.^{2} = total cross area of bars

fy = 73 ksi

Therefore:

$F_{nt} = 6.28 * 73 = 458.7$ kips

P_{tie} = load carried by the tie (see figure 4.7)

$P_{tie} = (12/93) * \tan(\theta) * P_n = F_{nt} = 458.7$ kips

$P_n = 358.9$ kips

The same procedure is followed to evaluate F_{nt} and P_n for the ties of the other beams.

As can be seen in Table 4.1, nodal zones or ties were not critical for the test specimens. Accordingly, nodal zone failure was not observed during the tests. Nominal loads (P_n) required to fail nodal zones were greater than the maximum loads applied during the tests (P_{test}), except for tests eight and nine. The high compressive strength of the nodal zones seen in test 8 and 9 is due primarily to the tri-axial stresses developed within the node due to confinement from the struts and bearing plates. This stress state enhances the ultimate strength of concrete.

Table 4.1 Capacities of test specimens: ACI 318-02 predictions vs experiments

	A		B		C		Strut 1		Strut 2		Ties			
Test	F_{nn}	P_n	F_{nn}	P_n	F_{nn}	P_n	F_{ns}	P_n	F_{ns}	P_n	F_{nt}	P_n	P_{test}	P_{test} / P_n
1	180.5	232.9	349.3	1552.6	436.7	436.7	154.3	103.3	129.3	99.6	458.7	358.9	130.6	1.31
2	209.5	270.4	349.2	1552.0	436.5	436.5	154.3	103.2	129.2	99.6	458.7	358.9	140.2	1.41
3	180.2	232.6	348.8	1550.4	436.1	436.1	154.1	103.1	129.1	99.5	458.7	358.9	194.9	1.96
4	211.5	272.9	352.5	1566.7	440.6	440.6	194.7	130.3	163.1	125.7	458.7	358.9	226.1	1.80
5	182.1	249.5	352.5	1305.6	440.6	440.6	194.7	138.3	177.1	143.6	458.7	381.1	246.4	1.78
6	182.1	249.5	352.5	1305.6	440.6	440.6	155.7	110.6	141.7	114.9	458.7	381.1	183.7	1.66
7	229.9	314.9	383.1	1418.9	478.9	478.9	169.2	120.2	154.0	124.8	458.7	381.1	146.2	1.22
8	196.5	253.5	633.8	2817.0	792.3	792.3	350.0	234.2	293.2	226.0	802.7	628.1	367.7	1.57
9	225.9	302.2	728.7	2671.9	910.9	910.9	402.4	286.9	368.0	299.2	802.7	669.4	343.6	1.20
10	230.6	360.3	743.8	2066.1	929.7	929.7	410.7	332.8	439.6	394.3	802.7	760.6	230.2	0.69

Table 4.1 clearly shows that strengths of the struts controlled the strength of the beams tested in this study. As mentioned earlier, yielding of the flexural reinforcement, and hence tie failure was not observed in any of the test conducted.

As can be seen in Table 4.1 in nine of the ten tests ACI 318-02 provisions for STM provided safe estimates for the capacities of the beam specimens. As the ultimate strength of the "B-region" was reached first in test 10, failure load predictions for "D-regions" in this specimen are not meaningful. Hence, it is possible to conclude that for all specimens that failed in the D-regions load carrying capacities were predicted safety using ACI 318-02 provisions.

4.3 AASHTO LRFD BRIDGE DESIGN CODE'S STRUT AND TIE MODELING PROVISIONS

STM was recently implemented in AASHTO LRFD specifications. These specifications indicate that strut-and-tie models may be used to determine internal force effects near supports and the points of application of concentrated loads.

AASHTO LRFD specifications recommend that STM must be used when the distance between the center of applied loads and support reactions is less than twice the member thickness.

Once these regions are determined, a truss configuration is created based on the principal stress trajectories. Then, the dimensions of the struts, ties, and nodes that form this truss can be determined. Subsequently, strength of ties, nodes and struts can be checked to ensure safety. The strength of struts or ties can be calculated as follows:

The strength of struts or ties is based on:

$P_r = \phi * P_n$, where:

P_r = factored axial resistance of strut or tie.

ϕ = resistance factor for tension or compression

P_n = nominal axial resistance of a strut or tie

4.3.1.1 Strength of Struts

The nominal resistance of an unreinforced compressive strut can be determined as follows:

$$P_n = f_{cu} * A_{cs} \qquad \text{(Equation 4.8)}$$

where,

P_n = nominal resistance of compressive strut

f_{cu} = limiting compressive stress

$$f_{cu} = \frac{f'c}{0.8 + 170 * \varepsilon_1} \le 0.85 * f'_c \qquad \text{(Equation 4.9)}$$

f'_c = specified compressive strength of concrete 28 days

$$\varepsilon_1 = \varepsilon_s + (\varepsilon_s + 0.002) * cot^2 \alpha_s \quad \ldots\ldots\ldots\ldots\ldots \quad \text{(Equation 4.10)}$$

ε_s = tensile strain in the concrete in the direction of the tension tie

α_s = the smallest angle between the compressive strut and adjoining tension ties (deg)

A_{cs} = effective cross-sectional area of strut

The geometry of a strut is a function of the dimension of the bearing plate (l_b), the tie width (h_a), the diameter of the transverse steel (d_{ba}), the angle of inclination of the strut, (Figure 4.8) as weel as the arrangement of transverse ties (Figure 4.9).

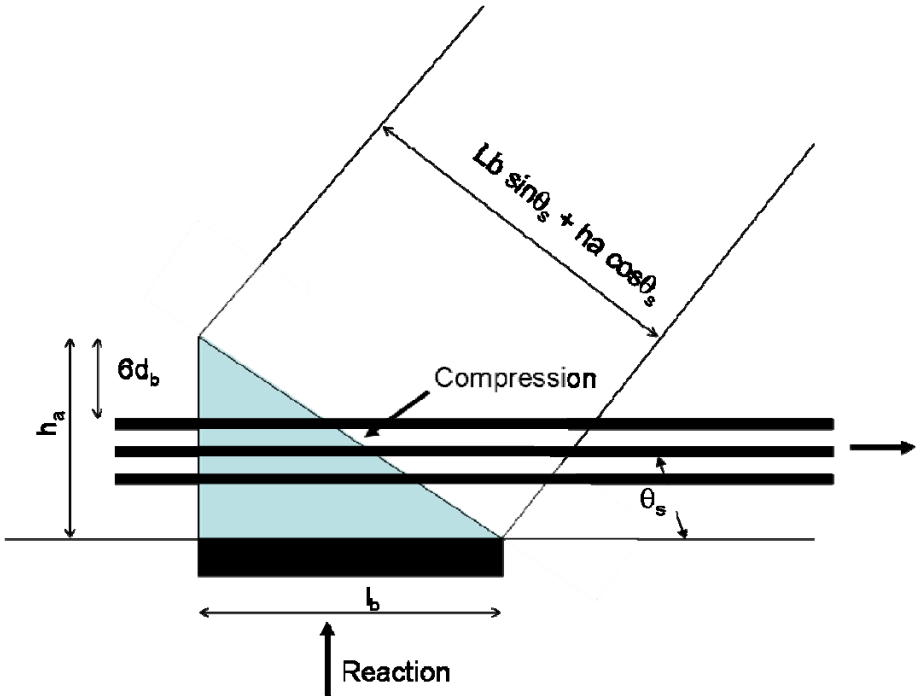

Figure 4.8 Strut, Tie and node geometry as per AASHTO LRFD specifications

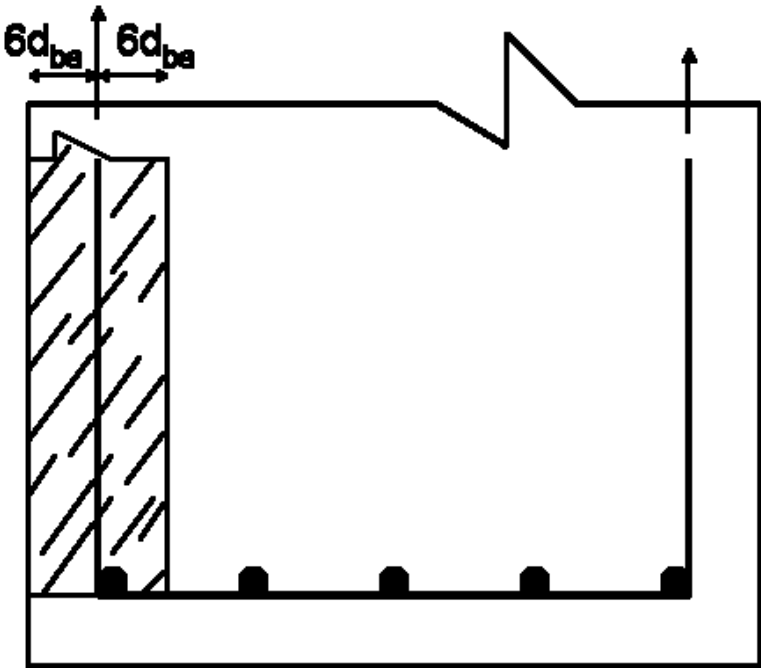

Figure 4.9 Strut width as per AASHTO LRFD specifications

4.3.1.2 Strength of Ties

The nominal resistance of a tension tie is:

$P_n = fy * A_{st}$ excluding Prestressed reinforcement (Equation 4.11)

P_n = nominal resistance of tension tie

fy = specified minimum yield strength of reinforcing bars

Ast = area of nonprestressed reinforcement in a tie

4.3.1.3 Strength of Nodal Zones

AASHTO LRFD specifications indicate that the concrete compressive stress in the node regions shall not exceed the concrete compressive strength of nodes. Compressive strength of the nodes can be calculated as follows:

Compressive nodal strength = $0.85 \phi f'_c$ for nodes bounded by compressive struts and bearing areas

Compressive nodal strength = 0.75 ϕ f'$_c$ for nodes anchoring one tension tie

Compressive nodal strength = 0.65 ϕ f'$_c$ for nodes anchoring more than one tension tie

where,

f'$_c$ = specified compressive strength of concrete at 28 days

ϕ = resistance factor for tension or compression

4.3.2 Calculations and Observations

Designers usually choose ε_s as the yield strain (ε_y) in Equation 4.10. Accordingly ε_s = 0.00207 is used to calculate ε_1 in Equation 10 for concrete capacity bars. In addition the strain readings obtained from the strain gages on the reinforcing bars during testing (ε_{test}) will also be used to determine the effect of using $\varepsilon_s = \varepsilon_y$ in design.

AAHSTO LRFD indicates that ε_s varies over the width of a strut-and-that it is appropriate to use the value at the center line of the strut. Therefore, the values of the afore mentioned strains (ε_y and ε_{test}) at the centerline of the strut will also be considered for the following calculations.

4.3.2.1 Nodal zones

The following three forces were determined for the nodal zones:

F_{nn} = nominal strength of node at a face of a nodal zone

$P_{n\ allowable}$ = nominal force of specimen at failure of nodal zone

P_{test} = load at failure of specimen registered from test

An example of calculation of strength of nodal zone A of Test 1 (Figure 4.5) is shown next:

Concrete compressive stress capacity = 0.75 * f'c for nodes anchoring a tension tie.

A_c = area limited by the bearing plates =15.5"*6"= 93 in^2

F_{nn} = Ac*0.75 * f'c

F_{nn} = 93*0.75*2.854 = 199.1 kips

(93/120) $P_{n\ allowable}$ = F_{nn} = 199.1 kips

$P_{n\ allowable}$ = 256.9 kips (see Figure 4.5)

The same procedure is followed to evaluate F_{nn} and $P_{n\ allowable}$ of the other nodes (B and C) as well as the nodes of the other test specimens.

4.3.2.2 Struts

The following three forces were determined for the struts

P_n = nominal strength of a strut

$P_{n\ allowable}$ = nominal force of specimen at failure of strut

P_{test} = maximum load at failure of specimen obtained from test

An example of calculation of strength of strut 2 of specimen 1 is shown next:

$\theta_s = \tan^{-1}(d/a)$ = angle formed by the strut with respect to the horizontal

d =16.4 in. =distance from the center of the tension stresses to the extreme compression fiber.

a = 93 in. = shear span

$\theta_s = \tan^{-1}(16.4/93) = 0.17$ radians (10.0 degrees).

$h_a = \phi_{bar} + 6 * \phi_{bar} + cover + \phi_{stirrup}$ (see figure 4.8)

ϕ_{bar} = 1 in. Cover = 0.75 in. $\phi_{stirrup}$ = 3/8 in

$h_a = 1" + 6*1" + 3/4" + 3/8" = 8\ \frac{1}{8}$ in. = width of the tie

Depth of strut = $h_a * \cos(\theta) + lb * \sin(\theta)$

Depth of strut = $8.125 * \cos(9.98) + 10 * \sin(9.98) = 9.7$ in.

Width of strut = 2*($\phi_{stirrup}$ + cover + 6*ϕ_{bar})

width of strut = 2 * (3/4" + 3/8" + 6*1) = 14.25 in.

Effective cross section area of strut = 14.25" * 9.73" = 138.73 in^2.

$\varepsilon_s = 0.001259$ in/in = yielding strain of tie at center line of node

$$\varepsilon_1 = 0.0013 + (0.0013 + 0.002) * \cot^2(10.0)$$

$\varepsilon_1 = 0.1063$ in/in

$$f_{cu} = \frac{2.85}{0.8 + 170 * 0.11}$$

$f_{cu} = 0.15$ ksi

P_n = Effective area * f_{cu} = 21.0 Kips

P_{strut} = load carried by the strut = (12/93) * sin(θ) * $P_{n\ allowable}$

P_{strut} = 1.494 $P_{n\ allowable}$ = P_n = 21.0 kips (see figure 4.6)

$P_{n\ allowable}$ = 16.2 kips

The same procedure is followed to evaluate P_n and $P_{n\ allowable}$ of strut 2 and the other struts of the other beams.

4.3.2.3 Ties

The following three forces were determined for the tie

P_n = nominal resistance of tension tie

$P_{n\ allowable}$ = nominal force at failure of beam as a function of tie strength

P_{test} = load at failure of specimen obtained from test acting on a tie.

An example of calculation of the strength of the tie is shown next:

$Pn = A_s * fy$ $As = 6.28\ in.^2$ $fy = 73$ ksi

$Pn = 6.28 * 73 = 458.7$ Kips

P_{tie} = load carried by the tie = =(12/93) * tan(θ) * $P_{n\ allowable}$

1.278 $P_{n\ allowable}$ = Pn = 458.7 kips

$P_{n\ allowable}$ = 358.9 kips

The same procedure is followed to evaluate P_n and $P_{n\ allowable}$ for the ties of the other beams.

Table 4.2 Summary of strengths of every element of every test (kips)

	Node A		Node B		Node C		Strut 1		Strut 2		Tie		
Test	F_{nn}	P_n allowable	F_{nn}	P_n allowable	F_{nn}	P_n allowable	P_n	P_n allowable	P_n	P_n allowable	P_n	P allowable	P_{test}
1	199.1	256.9	385.3	1712.4	436.7	436.7	162.3	108.6	21.0	16.2	458.7	358.9	130.6
2	231.1	298.2	385.2	1711.8	436.5	436.5	162.3	108.6	21.0	16.2	458.7	358.9	140.2
3	198.8	256.5	384.8	1710.0	436.1	436.1	162.1	108.5	20.9	16.1	458.7	358.9	194.9
4	233.3	301.0	388.8	1728.0	440.6	440.6	163.8	109.6	21.2	16.3	458.7	358.9	226.1
5	200.9	275.2	388.8	1851.4	440.6	440.6	163.8	116.4	34.5	28.0	458.7	381.1	246.4
6	200.9	275.2	388.8	1440.0	440.6	440.6	163.8	116.4	34.5	28.0	458.7	381.1	183.7
7	253.5	347.3	422.6	1565.0	478.9	478.9	178.0	126.5	37.5	30.4	458.7	381.1	246.4
8	216.7	279.6	699.1	3107.0	792.3	792.3	176.7	118.2	22.8	17.6	802.7	628.1	367.7
9	249.1	342.6	482.2	1768.1	546.5	546.5	203.2	144.9	44.0	35.8	802.7	669.4	343.6
10	254.3	397.4	492.2	1367.3	557.8	557.8	203.2	144.9	98.2	88.1	802.7	760.6	230.2

Nodal zone failure was not observed in any of the tests, which is consistent with the high capacities of the nodes (F_{nn}) (Table 4.2). Except for tests eight and nine were $P_{n,\ allowable}$ was smaller than $P_{test.}$

In these tests (8 and 9) nodal zone A was the most critical node with bearing plates that did not cover the entire area of the bottom of the beam. These bearing plates were used to support the forces at the assumed struts developed at the sides of a beam section as per AASHTO provisions (see Figure 4.9). Therefore, the area of the bearing plates was small enough to only support a nominal force ($P_{n\ allowable}$) that was lower than the failure load (P_{test}).

Not having failures in nodal zone A as predicted by AASTHO inn tests 8 and 9 indicates that either the compressive strength of the concrete at that region is enhanced by the confinement provided by the bearing plates or the struts are developed in an area

beyond the limits established by six times the diameter of the longitudinal reinforcement (Figure 4.9).

The capacity of strut 2 controlled the maximum load capacity for each test specimen. In addition, very large differences between the experimental and predicted capacities can be observed in Table 4.3.

Table 4.3 Experimental vs. Predicted capacities ($P_{test}/P_{n\ allowable}$)

Test	P_n	$P_{n\ allowable}$	P_{test}	$P_{test}/P_{n\ allowable}$
1	21.0	16.2	130.6	8.08
2	21.0	16.2	140.2	8.68
3	20.9	16.1	194.9	12.08
4	21.2	16.3	226.1	13.86
5	34.5	28.0	246.4	8.80
6	34.5	28.0	183.7	6.56
7	37.5	30.4	246.4	8.10
8	22.8	17.6	367.7	20.90
9	44.0	35.8	343.6	9.60
10	98.2	88.1	230.2	2.61

The large differences observed between the predicted and experimental capacities are attributed to the following factors:

(i) As the test specimens were loaded asymmetrically, shallow struts governed the capacity in all the tests. In such cases the permissible stresses obtained through the use of AASHTO LRFD specifications are rather low.

(ii) Strut width is limitations shown in Figure 4.9 had significant implications in establishing the effective strut areas and hence the capacity of the test specimens.

In order to investigate the need to limit the strut widths, as shown in Figure 4.9, the capacities of the struts are recalculated using the full member widths. As can be seen in the Table 4.4 the use of AASHTO provisions for permissible strut stresses in

conjunction with full member width provide safe estimates for the member capacities and reduce the unnecessary levels of conservatism.

Table 4.4 The influence of strut width on member capacities (kips)

P_n (AAHSTO)	P_n (AAHSTO)	P_n (width of beam)	P_{test}	P_{test} / $P_{n\ all\ width}$
8	17.59	37.04	367.69	9.93
9	35.80	75.37	343.60	4.56
10	88.12	185.51	230.22	1.24

In order to investigate the impact of using yield strain in obtaining the permissible strut stresses, experimentally evaluated strains are used in capacity estimates. These estimates are then compared with the conventional calculations where steel strain is taken as yield strain. As can be seen in Table 4.5 the use of εy (rather than the strain measured during the tests) reduces the nominal capacities by about 20%. This certainly adds to the excessive conservatism of the AASHTO LRFD specifications for STM.

Table 4.5 Nominal loads at εy and ε_{test}

	$P_{n\ allowable}$			
Test	$P_n\ \varepsilon_y$ (kips)	$P_n\ \varepsilon_{test}$ (kips)	P_{test} (kips)	$P_n(\varepsilon_y)$ /P_n (ε_{test})
1	16.2	20.2	130.6	0.801
2	16.2	20.2	140.2	0.801
3	16.2	20.1	194.9	0.801
4	16.3	20.3	226.1	0.801
9	43.4	53.9	343.6	0.804
10	141.0	173.4	230.2	0.813

If reinforcing bars strains at the centerline of the compressive struts are used in capacity estimations, the nominal capacities of the struts (and hence the beams) increase by about 35-40% (Table 4.6). Hence it is clear that selection o the strain has important

implications on predicted strength values. Conversely, the use of yield strain in estimating the permissible stresses in struts may result in overly conservative designs that may not be possible to implement in some occasions.

Table 4.6 Nominal capacity calculations using strain at the centerline of struts

Test	P_n (not at centerline) (kips)	P_n (at centerline) (kips)	Pn center / Pn not center
1	11.7	16.2	1.38
2	11.7	16.2	1.38
3	11.7	16.1	1.38
4	11.8	16.3	1.38
5	20.4	28.0	1.37
6	20.4	28.0	1.37
7	22.2	30.4	1.37
8	12.8	17.6	1.38
9	26.1	35.8	1.37
10	65.0	88.1	1.36

CHAPTER 5
Conclusions

The following conclusions can be reached based on this research study:

- Strut-and-tie modeling is a powerful technique that can be used to design D-regions of structural members.
- Both AASHTO LRFD Bridge Design Specifications and ACI 318-02 provide safe estimates for the load carrying capacities of the test specimens
- AASHTO LRFD Bridge Design Specifications provide overly conservative strength predictions. This is primarily due to the restrictive nature of the AASHTO Specification's provisions for strut widths and permissible stresses for shallow strut angles.
- Based on the ten tests conducted on seven beams, it can be concluded that full widths of the members can be used to calculate strut capacities.
- The use of yield strain in establishing the permissible strut stresses (AASHTO LRFD Bridge Design specifications) appears to be a safe assumption. However, for the specimens tested in this study such a safe estimation of the reinforcing bar strain at the centerline of a strut resulted in excessive levels of conservatism.

REFERENCES

1. ACI 318 2002: Building Code Requirements for Structural Concrete Code and Commentary, American Concrete Institute, Farmington Hills, MI.

2. AAHSTO LRFD Bridge Design Specifications, American Association of State Highway Transportation Officials, 444 North Capitol Street, N. W. Suite 249, Washington, D.C., 2001, ISBN: 1-56061-194-3, Second Edition, 1998.

3. Schalaich, Schäfer, Jennewein 1987: J. Schalaich, K Schäfer, M. Jennewein, Toward a Consistent Design of Structural Concrete, PCI Journal, Prestressed Concrete Institute, Vol. 32, No. 3, May-June 1987, pp. 74-150.

4. Hagenberger, Breen 2002: B. Chen, M. Hagenberger, J. E. Breen, Evaluation of Strut-and-Tie Modeling Applied to Dapped Beam with Opening, ACI Structural Journal Julay-August 2002, Technical Paper Tile no. 99-S46,

5. Marti 1985: P. Marti, Basic Tools of Reinforced Concrete Beam Design, ACI Journal January-February 1985, Technical Paper Title no. 82-4.